

# Nonlinear mixed convective nanofluid flow along moving vertical rough plate

P.M. Patil\* and M. Kulkarni

*Department of Mathematics, Karnatak University, Pavate Nagar, Dharwad - 580003, India.*

*e-mail: pmpmath@gmail.com; mgkmaths@gmail.com*

Received 16 July 2019; accepted 19 September 2019

The objective of the current research paper is to investigate the effects of surface roughness on magnetohydrodynamic nonlinear mixed convection nanofluid flow over vertically moving plate. The highly coupled dimensional nonlinear partial differential equations (NPDE) are converted into dimensionless NPDE along with the boundary conditions with the help of non-similar transformations. The resulting set of dimensionless nonlinear PDE's are solved by using the Quasilinearization technique and implicit finite difference method. Impacts of various dimensionless parameters, namely, Brownian diffusion ( $Nb$ ), nonlinear mixed convection ( $\gamma$ ), nanoparticle buoyancy ratio ( $Nr$ ), Lewis number ( $Le$ ), thermophoresis ( $Nt$ ), frequency ( $n$ ), magnetic ( $M$ ), and small parameter ( $\alpha$ ) are studied in detail on profiles as well as gradients. The results reveal that increasing values of  $\gamma$  increase the velocity profile, while increasing values of  $Nr$  decrease the same. Further, increasing values of  $\alpha$  and  $n$  exhibit sinusoidal variations on skin-friction coefficient, heat, and nanoparticle mass transfer rates. Moreover, the presence of nonlinear mixed convection parameter has significant effects on fluid flow compared to its absence. In addition to this, rate of heat transfer is analyzed in presence and absence of nanoparticles.

**Keywords:** Magnetohydrodynamic flow; moving plate; nanofluid; nonlinear mixed convection; quasilinearization technique; surface roughness.

PACS: 44.20.+b; 44.05.+e; 44.25.+f; 47.11.Bc; 47.15.cb; 47.35.Tv

DOI: <https://doi.org/10.31349/RevMexFis.66.153>

## 1. Introduction

Many researchers have investigated linear variations in the temperature as well as density relations. The study of nonlinear variations in temperature and density relation [1-4] is a new idea to analyze the impacts of thermo-physical properties, such as temperature variations, viscous dissipation, density variations, etc. In such cases, nonlinearity plays a vital role and applications can be seen in the engineering and industrial applications. Some of these are, for example, thermal systems, combustion, geothermal power, reactor safety, electronics cooling, solar collectors, and drying surfaces, which exhibit the nonlinearity phenomenon in temperature and density variations when operating at high temperatures[1-3]. The nonlinearity term has been considered in the buoyant force due to its notable physical significance on fluid flow and heat transport properties of fluids.

Sinha [1] has studied the frictional heating system effects and heat sources on convective flows along with the varying density in terms of quadratic temperature difference. Vajravelu and Sastri [2] have investigated the wall heat transfer between vertical walls in presence and absence of nonlinear density temperature variations. Motsa *et al.* [3] have investigated the impact of nonlinear temperature as well as density variations on nanofluid flow over the convective vertical surface. In the work of [3], the governing nonlinear PDE's are numerically solved by the spectral linearization technique and their results reveal that higher values of thermophoresis parameter and nonlinear temperature enhance the magnitude of the velocity profile. Bandaru *et al.* [4] have inspected the impact of nonlinear convection and the thermophoretic coefficient on a rotating fluid due to a rapid rotating cone and their results reveal that the increasing values of nonlinear

temperature, as well as concentration, increase the magnitude of surface-friction, Nusselt number, and Sherwood number significantly. Further, Mandal and Mukhopadhyay [5] have examined the effects on micropolar fluid flow over exponentially stretching sheet in presence and absence of nonlinear convection and their results show that the velocity profile increases for the presence of both nonlinear and mixed convection parameters.

Surface roughness [6] can be defined as the small irregularities on surface texture that are an integral part of a material or the production of the materials. The study of surface roughness has many applications in the area of science and technology, namely, electronic cooling devices, heat transfer exchangers, production of polymers and nuclear reactor cooling, etc. [7-9]. Ehasn *et al.* [7] have studied the thermal and hydro-kinematic properties of water-based alumina nanofluid flow between two parallel rough plates. Salimpour *et al.* [8] have studied rate of heat transfer on iron oxide/de-ionized with water as base fluid and also with the Cu surface. Furthermore, their study reveals that boiling stagnation point increases heat transfer rate for both rough and smooth surfaces with high heat flux. Influence of roughness and convective heat transfer flow on the boundary surface was studied by Pan *et al.* [9]. In their study, numerical simulation was carried out by COMSOL5.3 and their results indicate that the drag of liquid increases the surface roughness, significantly.

The suspension of nanometer sized metallic particles in base fluid yields the nanofluid. The term “nanofluid” was coined by Choi and Eastman [10] in 1995. The nanoparticles are formed by several materials such as metal oxides, ceramics, semiconductors, or alloyed nanoparticles etc. Nanofluids have gained great attention due to their controlling and en-

hancing of heat transport properties that make them suitable for engineering and industrial purposes such as solid-state lighting, power generation, microfluidics, cancer treatment, nuclear reactor cooling, heat exchangers, etc. [10-12]. Recently, Subhashini and Sumathi [11] have studied the effects of mixed convective nanofluid flow over a vertically moving plate with three different nanoparticles, namely, Copper, Aluminium Oxide, and Titanium Oxide along with water as the base fluid. Sheikholeslami *et al.* [12] have investigated the convective heat transfer by a magneto nanofluid with water as the base fluid in a three-dimensional enclosure. Additionally, Ganesh Kumar *et al.* [13] have studied the heat transport characteristics on converging and diverging channel through water-based TiO<sub>2</sub> nanoparticles.

The above literature study points out that the effects of surface roughness and nonlinear mixed convection nanofluid flow is an advanced research approach and no attention has been given so far to study their effects. Thus, the aim of present paper is to study the Magnetohydrodynamics (MHD) nonlinear mixed convective nanofluid flow effects on surface roughness. In order to achieve the desired numerical accuracy, the obtained results are compared with the works of Minkowycz and Sparrow [14] and Mohamad *et al.* [15] for the various numerical values of *Ri* on heat transfer rate ( $Re^{-1/2}Nu$ ) in Table I. Minkowycz and Sparrow [14] have studied the local non-similarity solutions for boundary layer problem using non-similar solutions. Mohamad *et al.* [15] have investigated the impacts of thermal radiation on mixed convection magnetohydrodynamic nanofluid flow past a moving plate. Further, the corresponding governing system of PDE's are solved with the help of local linearization method, Runge-Kutta method of fourth order (RK4) and the shooting technique. In the current analysis, governing equations are solved by using non-similar transformations, Quasi-linearization and the implicit finite difference method [16-19]. Thus, the obtained numerical results are validated with the works of [14] and [15] in the limiting case of  $\xi = 0$ , when  $Pr = 0$ ,  $Re = 0$ ,  $Nb = 0$ ,  $Ec = 0$ ,  $M = 0$ ,  $Le = 0$ ,  $Nt = 0$ ,  $\varepsilon = 0$ ,  $Nr = 0$ ,  $\alpha = 0$ ,  $n = 0$ , and  $\gamma = 0$ . The comparison shows that the obtained results are in good agreement with the previously established results.

## 2. Mathematical formulation

In the present problem, a steady, laminar nonlinear mixed convection nanofluid flow along moving vertical rough plate is considered. The plate is taken along the *x*-axis and *y*-axis is measured perpendicular to the plate as shown in Fig. 1. The surface roughness is assumed to be along the plate and is modeled in terms of sine waveform of small amplitude and high frequency. The surface roughness is modelled through a deterministic approach [20].

The velocity of the plate is taken as  $U_0(x)$ , while that of the free stream is taken as  $U_\infty(x)$ . The temperature of the moving plate is more than that of ambient fluid ( $T_w > T_\infty$ ), where,  $T_w$  and  $T_\infty$  are the wall temperature and ambient fluid

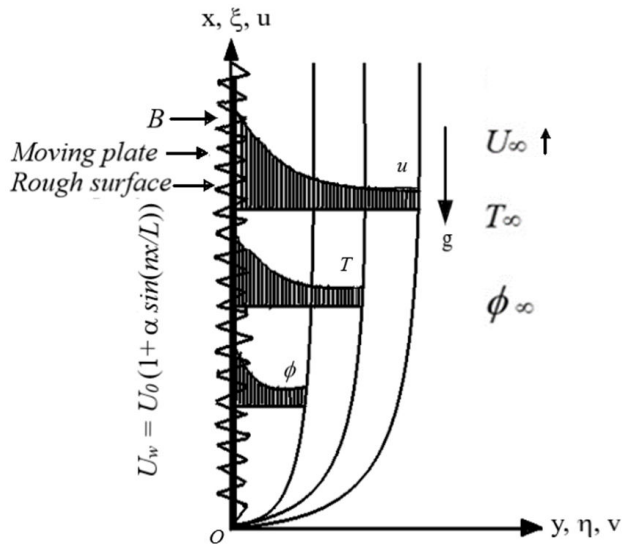


FIGURE 1. Flow geometry and co-ordinate system.

temperature, respectively. Here,  $\phi_w$  and  $\phi_\infty$  indicate the nanoparticle volume fraction at the wall and away from the surface, respectively. The nonlinear temperature variations are considered in the buoyancy force term, and the density variations are modelled through Boussinesq approximation [21-23]. In the Buongiorno two-phase model, every particle has an independent existence in the carrier liquid, which possibly gives rise to several slip mechanisms. Among these mechanisms, thermophoresis and Brownian diffusion effects are dominant in the absence of turbulent flow, and hence, we have considered these effects in the present analysis by employing the former model [24]. Thus, the suitable governing equations are [3,25-28].

Continuity equation:

$$\frac{\partial u}{\partial x} + \frac{\partial v}{\partial y} = 0, \tag{1}$$

Momentum equation:

$$u \frac{\partial u}{\partial x} + v \frac{\partial u}{\partial y} = \nu \frac{\partial^2 u}{\partial y^2} + \frac{\sigma B_0^2}{\rho} (U_\infty - u) + (1 - \phi_\infty)g \times [\beta_0(T - T_\infty) + \beta_1(T - T_\infty)^2] - g \left( \frac{\rho_p - \rho}{\rho} \right) (\phi - \phi_\infty), \tag{2}$$

Energy equation:

$$u \frac{\partial T}{\partial x} + v \frac{\partial T}{\partial y} = \alpha_m \frac{\partial^2 T}{\partial y^2} + \frac{\sigma B_0^2}{\rho C_{n,f}} (U_\infty - u) + \frac{\rho_p C_{pp}}{\rho C_{n,f}} \left( \frac{D_T}{T_\infty} \left( \frac{\partial T}{\partial y} \right)^2 + D_B \frac{\partial \phi}{\partial y} \frac{\partial T}{\partial y} \right). \tag{3}$$

Nanoparticle volume fraction equation:

$$u \frac{\partial \phi}{\partial x} + v \frac{\partial \phi}{\partial y} = D_B \frac{\partial^2 \phi}{\partial y^2} + \frac{D_T}{T_\infty} \frac{\partial^2 T}{\partial y^2}. \tag{4}$$

with the corresponding boundary conditions given by

$$\begin{aligned}
 y = 0 : \quad u &= U_w(x) = U_0 \left( 1 + \alpha \sin \left( \frac{nx}{L} \right) \right), \\
 v &= 0, \quad T = T_w, \quad \phi = \phi_w, \\
 y \rightarrow \infty : \quad u &\rightarrow U_\infty, \quad T \rightarrow T_\infty, \quad \phi \rightarrow \phi_\infty, \quad (5)
 \end{aligned}$$

where  $x$  and  $y$  are the distances along  $x$  and  $y$  co-ordinates,  $u$  and  $v$  are the velocity component along  $x$  and  $y$  axes,  $U_0$  is the reference velocity,  $U_w$  is the wall velocity,  $U_\infty$  is free stream velocity,  $B_0$  is the magnetic field strength,  $\sigma$  is electrical conductivity of the fluid,  $\beta_0$  and  $\beta_1$  represent the linear and nonlinear thermal expansion coefficients of nanofluid,  $g$  is the acceleration due to gravity,  $\rho$  is the density of nanofluid,  $\rho_p$  is the nanoparticle mass density,  $\alpha_m$  is the thermal diffusivity of nanofluid,  $\phi$  is nanoparticle volume fraction,  $\phi_w$  and  $\phi_\infty$  are the nanoparticle volume fraction at the wall and ambient conditions,  $T$  is the temperature,  $T_w$  and  $T_\infty$  denote the temperature at the wall and ambient conditions,  $D_B$  is the Brownian diffusion coefficient,  $D_T$  is thermophoretic coefficient,  $\rho_p C_{pp}$  represents the heat capacity of nanoparticles,  $\rho C_{nf}$  denotes the heat capacity of nanofluid,  $\alpha$  is the small parameter, and  $n$  is the frequency parameter.

Non-similar transformations:

$$\begin{aligned}
 \xi &= \frac{x}{L}, \quad \eta = y \sqrt{\left( \frac{U_0}{vx} \right)}, \quad f_n = F, \\
 \psi(x, y) &= \sqrt{(vU_0x)} f(\xi, \eta), \\
 T - T_\infty &= (T_w - T_\infty) G(\xi, \eta), \\
 \phi - \phi_\infty &= (\phi_w - \phi_\infty) S(\xi, \eta), \\
 u &= \frac{\partial \psi}{\partial y}, \quad v = -\frac{\partial \psi}{\partial x}. \quad (6)
 \end{aligned}$$

With the application of Eq. (6), (1) satisfied identically and the Eqs. (2)-(4), are as follows:

$$\begin{aligned}
 F_{\eta\eta} + \left\{ \frac{f}{2} + \xi f_\xi \right\} F_\eta - \xi F_\xi F + \xi M^2 Re(\varepsilon - F) \\
 + \xi RiG(1 + \gamma G) - \xi RiNrS = 0, \quad (7)
 \end{aligned}$$

$$\begin{aligned}
 G_{\eta\eta} + Pr \left\{ \frac{f}{2} + \xi f_\xi \right\} G_\eta + Pr Nb S_\eta G_\eta + Pr Nt G_\eta^2 \\
 + \xi Pr Re Ec M^2 (\varepsilon - F)^2 = 0, \quad (8)
 \end{aligned}$$

$$S_{\eta\eta} + Le \left\{ \frac{f}{2} + \xi f_\xi \right\} S_\eta - \xi Le S_\xi F + \frac{Nt}{Nb} G_{\eta\eta} = 0. \quad (9)$$

The non-dimensional boundary conditions are

$$\begin{aligned}
 F = 1 + \alpha \sin(n\xi), \quad G = 1, \quad S = 1 \quad \text{at} \quad \eta = 0, \\
 F \rightarrow \varepsilon, \quad G \rightarrow 0, \quad S \rightarrow 0 \quad \text{as} \quad \eta \rightarrow \infty. \quad (10)
 \end{aligned}$$

In this analysis,  $F$  is the dimensionless velocity,  $G$  is the dimensionless temperature,  $S$  denotes dimensionless nanoparticle volume fraction,  $f$  is the non-dimensional

stream function,  $\xi$  and  $\eta$  are the transformed variables,  $\psi$  is the stream function,

$$Nr = \left( \frac{\rho_p - \rho}{\rho} \right) \frac{(\phi_{w_0} - \phi_\infty)}{\beta_0(T_w - T_\infty)} \frac{1}{(1 - \phi_\infty)}$$

denotes the nanoparticle buoyancy ratio parameter,  $Pr = v/\alpha_m$  represents the Prandtl number,  $\varepsilon = U_\infty/U_0$  is the velocity ratio parameter,  $M = B_0/[U_0(\sqrt{\sigma v/\rho})]$  is the Magnetic parameter,  $Ec = U_0^2/[C_{nf}(T_w - T_\infty)]$  denotes the Eckert number (viscous dissipation parameter),  $\gamma = \beta_1/\beta_0(T_w - T_\infty)$  represents the nonlinear mixed convection parameter,  $Le = v/D_B$  is the Lewis number,  $Ri = Gr/Re^2$  denotes the Richardson number,  $Re = U_0L/v$  is the Reynolds number,

$$Gr = \frac{g\beta_0(1 - \phi_\infty)(T_w - T_\infty)L^3}{v^2}$$

is the Grashof number,  $Nb = JD_B[(\phi_w - \phi_\infty)/v]$  and  $Nt = JD_T[(T_w - T_\infty)/vT_\infty]$  are the Brownian diffusion parameter and thermophoresis parameter, respectively. where,  $J$  is the ratio between heat capacity of nanoparticles to the heat capacity of the nanofluid  $J = \rho_p C_{pp}/\rho C_{nf}$  Kindly include comma instead of full stop.

$$f(\xi, \eta) = \int_0^\eta F d\eta + f_w, \quad (11)$$

where  $f_w = 0$ , represents an impermeable surface.

The gradients defined at the wall are as below:

Skin friction coefficient:

$$\begin{aligned}
 C_f = \frac{2v \left( \frac{\partial u}{\partial y} \right)_{y=0}}{U_w^2} = 2\sqrt{(\xi Re)} \\
 \times (1 + \alpha \sin(\xi))^{-2} F_\eta(\xi, 0), \quad (12)
 \end{aligned}$$

or  $Re^{-1/2} C_f = 2F_\eta(\xi, 0)\sqrt{\xi}(1 + \alpha \sin(\xi))^{-2}$ .

Heat transfer rate:

$$Nu = -x \frac{\left( \frac{\partial T}{\partial y} \right)_{y=0}}{(T_w - T_\infty)} = -G(\xi, 0)\sqrt{(\xi Re)}, \quad (13)$$

or  $Re^{-1/2} Nu = -G_\eta(\xi, 0)\sqrt{\xi}$ ,

Nanoparticle mass transfer rate:

$$NSh = -x \frac{\left( \frac{\partial \phi}{\partial y} \right)_{y=0}}{(\phi_w - \phi_\infty)} = -S(\xi, 0)\sqrt{(\xi Re)}, \quad (14)$$

or  $Re^{-1/2} NSh = -S_\eta(\xi, 0)\sqrt{\xi}$ .

### 3. Method of solution

The Quasilinearization technique is used to solve the system of nonlinear non-dimensional PDE from Eqs. (7)-(9) with appropriate boundary constraints (10) and the resultant set of equations are given below:

$$F_{\eta\eta}^{i+1} + A_1^i F_{\eta}^{i+1} + A_2^i F_{\eta}^{i+1} + A_3^i F_{\xi}^{i+1} + A_4^i G^{i+1} + A_5^i S^{i+1} = A_6^i, \quad (15)$$

$$G_{\eta\eta}^{i+1} + B_1^i G_{\eta}^{i+1} + B_2^i G_{\xi}^{i+1} + B_3^i F^{i+1} + B_4^i S_{\eta}^{i+1} = B_5^i, \quad (16)$$

$$S_{\eta\eta}^{i+1} + C_1^i S_{\eta}^{i+1} + C_2^i S_{\xi}^{i+1} + C_3^i F^{i+1} + C_4^i G_{\eta\eta}^{i+1} = C_5^i, \quad (17)$$

where coefficient functions at the  $i^{th}$  iterative index are known and that at  $(i + 1)^{th}$  are to be find out.

The relevant boundary constraints are as given below:

$$F^{i+1} = 1 + \alpha \sin(n\xi), \quad G^{i+1} = 1, \quad S^{i+1} = 1, \quad \text{at } \eta = 0.$$

$$F^{i+1} = \varepsilon, \quad G^{i+1} = 0, \quad S^{i+1} = 0, \quad \text{at } \eta = \eta_{\infty}. \quad (18)$$

where  $\eta_{\infty}$  is the edge of boundary layer.

The coefficients in Eqs. (15)-(17) are

$$A_1^i = \left\{ \frac{f}{2} + \xi f_{\xi} \right\}; \quad A_2^i = -\xi(F_{\xi} + M^2 Re);$$

$$A_3^i = -\xi F; \quad A_4^i = \xi Ri(1 + 2\gamma G); \quad A_5^i = -\xi Ri Nr;$$

$$A_6^i = -\xi(M^2 Re \varepsilon + F_{\xi} F - Ri \gamma G^2);$$

$$B_1^i = Pr \left\{ \frac{f}{2} + \xi f_{\xi} \right\} + 2Pr Nt G_{\eta} + Pr Nb S_{\eta};$$

$$B_2^i = -\xi Pr F; \quad B_3^i = -(\xi Pr G_{\xi} + 2\xi Pr Re Ec M^2 (\varepsilon - F));$$

$$B_4^i = Pr Nb G_{\eta};$$

$$B_5^i = Pr Nt e^{2\xi} G_{\eta}^2 - \xi Pr G_{\xi} F + Pr Nb S_{\eta} G_{\eta} - \xi Pr Re Ec M^2 (\varepsilon^2 - F^2);$$

$$C_1^i = Le \left\{ \frac{f}{2} + \xi f_{\xi} \right\}; \quad C_2^i = -\xi Le F; \quad C_3^i = -\xi Le S_{\xi};$$

$$C_4^i = \frac{Nt}{Nb}; \quad C_5^i = -\xi Le F S_{\xi};$$

Equations (15)-(17), are discretized at each iteration step by using the formula of second-order central difference in boundary layer ( $\eta$ ) direction and the backward difference formula in the streamwise ( $\xi$ ) direction. For each iteration process, the results are in the form of block tri-diagonal matrix (BTDM). Then, BTDM computation has been carried by using Vargas's algorithm [29]. The step sizes  $\Delta\eta$  and  $\Delta\xi$  are

optimized and a convergence criterion is employed to guarantee the convergence of numerical solutions. Thus, when the difference between the present and previous iterations approaches the value lesser than  $10^{-4}$ , the iteration process is terminated.

That is,

$$\max \left\{ \left| (F_{\eta})_w^{i+1} - (F_{\eta})_w^i \right|, \left| (G_{\eta})_w^{i+1} - (G_{\eta})_w^i \right|, \left| (S_{\eta})_w^{i+1} - (S_{\eta})_w^i \right| \right\} < 10^{-4}. \quad (19)$$

### 4. Results and discussion

For the present problem, results are computed for the cases of absence and presence of a nonlinear mixed convection parameter, surface roughness, and nanoparticles. The values  $\gamma \neq 0$  and  $\gamma = 0$  indicate the presence and absence of nonlinear mixed convection parameter, respectively. Surface roughness is Modeled in terms of a small parameter  $\alpha$  along with the frequency parameter  $n$ . The value  $\alpha = 0$  indicates a smooth surface and  $\alpha \neq 0$  indicates a rough surface. The values  $Nr = 0.1$ ,  $Le = 10$ ,  $Nt = 0.1$ , and  $Nb = 0.1$  are taken in presence of nanoparticles, while these parameters are set to zero for the absence of nanoparticles [28]. The value of other parameters are taken as  $Pr = 7.0$ ,  $Ri = 10$ ,  $Re = 10$ ,  $\varepsilon = 0.5$ ,  $Ec = 0.1$ , [28]. The terms nanofluid and ordinary fluid indicate the base fluid with and without nanoparticles, respectively. The values  $M = 0$  and  $M \neq 0$  indicate the absence and presence of applied magnetic field.

#### 4.1. Velocity, temperature, and nanoparticle volume fraction profiles

Figure 2 portrays the effects of streamwise co-ordinate and non-similarity variable  $\xi$  on velocity profile  $F(\xi, \eta)$  and tem-

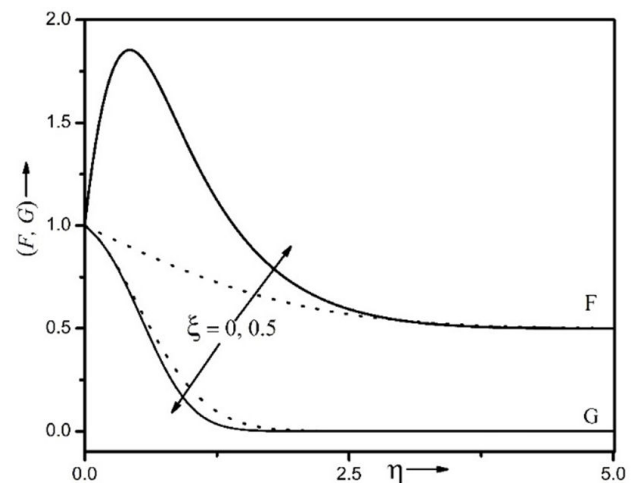


FIGURE 2. Effect of  $\xi$  on  $(F, G)$  for  $Pr = 7.0$ ,  $Ri = 10$ ,  $Le = 10$ ,  $Re = 10$ ,  $Nr = 0.1$ ,  $M = 0.1$ ,  $Nt = 0.1$ ,  $Ec = 0.1$ ,  $Nb = 0.1$ ,  $\varepsilon = 0.5$ ,  $\alpha = 0.5$ ,  $\gamma = 0.1$  and  $n = 50$ .

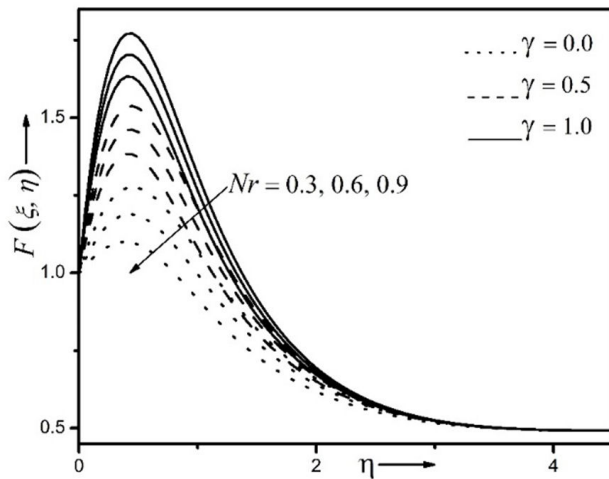


FIGURE 3. Effect of  $Nr$  and  $\gamma$  on  $F(\xi, \eta)$  for  $\xi = 0.5$ ,  $Pr = 7.0$ ,  $Le = 10$ ,  $Ri = 10$ ,  $Ec = 0.1$ ,  $Re = 10$ ,  $Nb = 0.1$ ,  $Nt = 0.1$ ,  $M = 0.1$ ,  $\varepsilon = 0.5$ ,  $\alpha = 0.5$ , and  $n = 50$ .

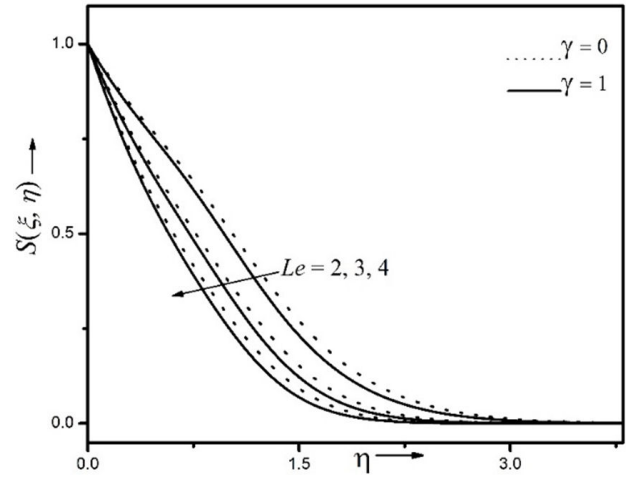


FIGURE 5. Effect of  $Le$  and  $\gamma$  on  $S(\xi, \eta)$  for  $\xi = 0.5$ ,  $Pr = 7.0$ ,  $Nb = 0.1$ ,  $Ri = 10$ ,  $Nt = 0.1$ ,  $Re = 10$ ,  $Nr = 0.1$ ,  $Ec = 0.1$ ,  $M = 0.1$ ,  $\varepsilon = 0.5$ ,  $\alpha = 0.5$ , and  $n = 50$ .

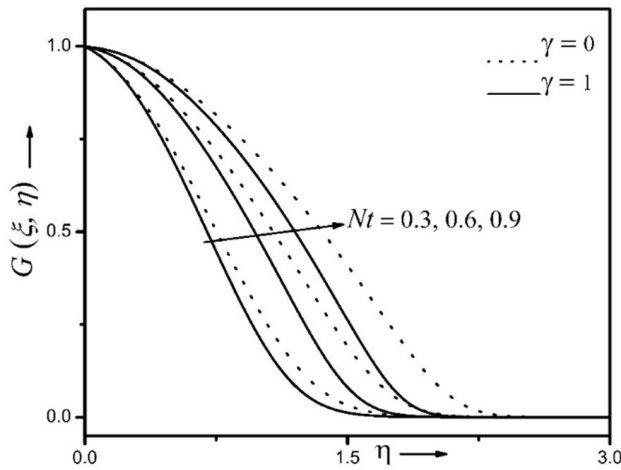


FIGURE 4. Effect of  $Nt$  and  $\gamma$  on  $G(\xi, \eta)$  for  $\xi = 0.5$ ,  $Le = 10$ ,  $Pr = 7.0$ ,  $Re = 10$ ,  $Ri = 10$ ,  $Nb = 0.1$ ,  $\varepsilon = 0.5$ ,  $M = 0.1$ ,  $Nr = 0.1$ ,  $Ec = 0.1$ ,  $\alpha = 0.5$ , and  $n = 50$ .

perature profile  $G(\xi, \eta)$  respectively. A small increase in the value of  $\xi$  enhances the magnitude of velocity profile, while reduces the temperature profile near the wall. The reason being is that the rising values of  $\xi$  act as a favourable pressure gradient on velocity profile while, the same rising values of  $\xi$  act as a negative pressure gradient on the temperature profile. Thus, increase in the magnitude of velocity profile  $F(\xi, \eta)$  and decrease in the magnitude of temperature profile  $G(\xi, \eta)$  is observed for non-zero values of  $\xi$ .

The influence of the nonlinear mixed convection parameter  $\gamma$ , thermophoresis parameter  $Nt$ , Lewis number  $Le$ , and nanoparticle buoyancy ratio parameter  $Nr$  on velocity  $F(\xi, \eta)$ , temperature  $G(\xi, \eta)$ , and nanoparticle volume fraction  $S(\xi, \eta)$  profiles are shown in Figs. 3-5. In particular, Fig. 3 displays the variations due to nonlinear mixed convection parameter  $\gamma$  and nanoparticle buoyancy ratio parameter  $Nr$  on velocity profile  $F(\xi, \eta)$ . The higher values of  $\gamma$  enhance the magnitude of the velocity profile. A reason for this

is that the rising values of  $\gamma$  rises the temperature of fluid, and which accelerates the fluid particles. Meanwhile, the larger values of  $Nr$  decrease the magnitude of velocity profile. The higher values of  $Nr$  reduces the buoyancy due to temperature in the nanofluid and this causes such variations in velocity profile.

The effects of nonlinear mixed convection parameter  $\gamma$  as well as thermophoresis parameter  $Nt$  on temperature profile  $G(\xi, \eta)$  are depicted in Fig. 4. The graph reveals that the larger value of  $Nt$  increases the magnitude of temperature profile, while an increase in the value of  $\gamma$  decreases the magnitude of temperature profile. This is due to fact that the thermophoresis force generated by the temperature gradient induces a faster movement of nanoparticles from the region of hot surface to cold surface and which drives the temperature of the fluid. Consequently, presence of nonlinear mixed convection ( $\gamma = 1$ ) reduces thermal boundary layer thickness, which in turn decreases the magnitude of the temperature profile.

Figure 5 displays the variations of  $Le$  and  $\gamma$  on nanoparticle volume fraction profile  $S(\xi, \eta)$ . The magnitude of nanoparticle volume fraction profile  $S(\xi, \eta)$  decreases for the larger values of Lewis number  $Le$  and nonlinear mixed convection parameter  $\gamma$ . For the higher values of  $Le$ , the Brownian diffusion is reduced whereas for increasing values of  $\gamma$ , the temperature difference between wall and fluid increases. These factors reduce the magnitude of nanoparticle volume fraction profile.

#### 4.2. Effect of Brownian diffusion and magnetic parameter on temperature profile and heat transfer rate

The Fig. 6 and Fig. 7 represent the variations of temperature profile  $G(\xi, \eta)$  as well as the Nusselt number or rate of heat transfer ( $Re^{-1/2}Nu$ ) for increasing values of Brownian diffusion parameter  $Nb$  and magnetic parameter  $M$ . For higher

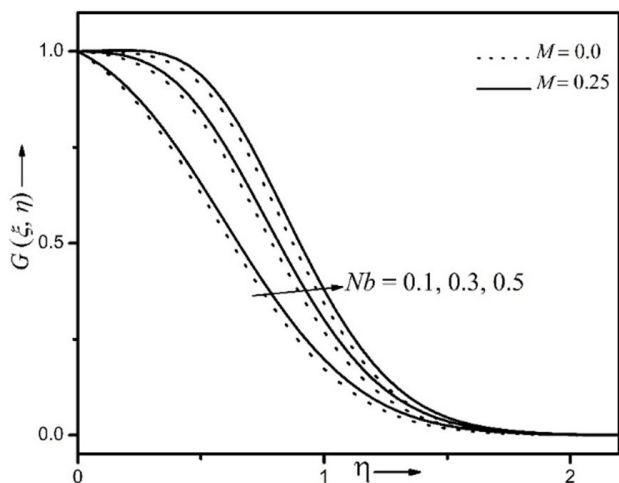


FIGURE 6. Effect of  $Nb$  and  $M$  on  $G(\xi, \eta)$  for  $\xi = 0.5$ ,  $Nt = 0.1$ ,  $Nr = 0.1$ ,  $Ri = 10$ ,  $Le = 10$ ,  $Re = 10$ ,  $Pr = 7.0$ ,  $Ec = 0.1$ ,  $\varepsilon = 0.5$ ,  $\gamma = 0.1$ ,  $\alpha = 0.5$ , and  $n = 50$ .

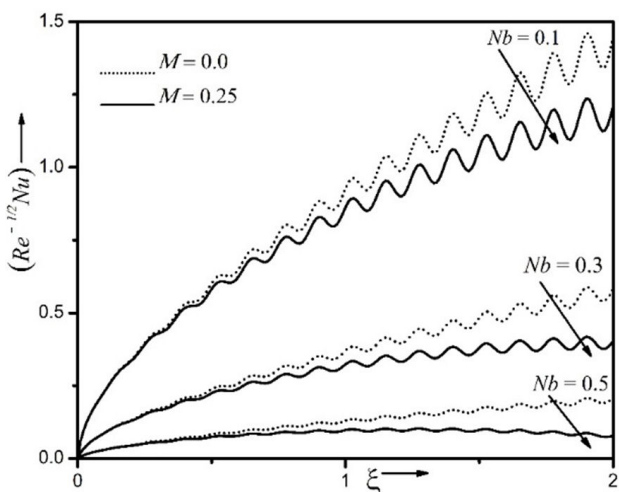


FIGURE 7. Effect of  $Nb$  and  $M$  on  $(Re^{-1/2}Nu)$  for  $Pr = 7.0$ ,  $Ri = 10$ ,  $Re = 10$ ,  $Le = 10$ ,  $Nr = 0.1$ ,  $Ec = 0.1$ ,  $Nt = 0.1$ ,  $\varepsilon = 0.5$ ,  $\alpha = 0.5$ ,  $n = 50$ , and  $\gamma = 0.1$ .

values of  $Nb$  and  $M$ , increase in the magnitude of temperature profile and decrease in heat transfer rate can be observed in the Fig. 6 and Fig. 7, respectively. A possible explanation is that an increase in values of  $Nb$  increases the random movement of nanoparticles from the hot plate to surrounding fluid and the nanoparticles penetrate deeper into the fluid. This enhances the temperature of the nanofluid. Consequently, the random motion of nanoparticles reduces their kinetic energy and this fact causes the a reduction in the heat transfer rate. On the other hand, the presence of magnetic parameter  $M$  increases the magnitude of the temperature profile and reduces the heat transfer rate. In presence of the magnetic parameter  $M$ , the Lorentz force opposes the movement of fluid particles and this fact causes such variations in the temperature profile as well as in heat transfer gradient.

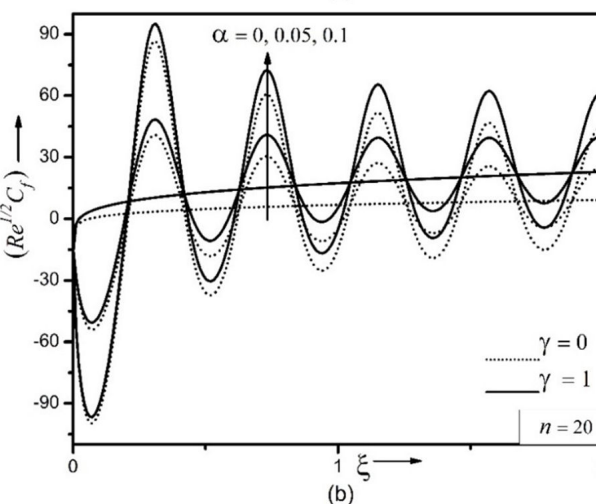
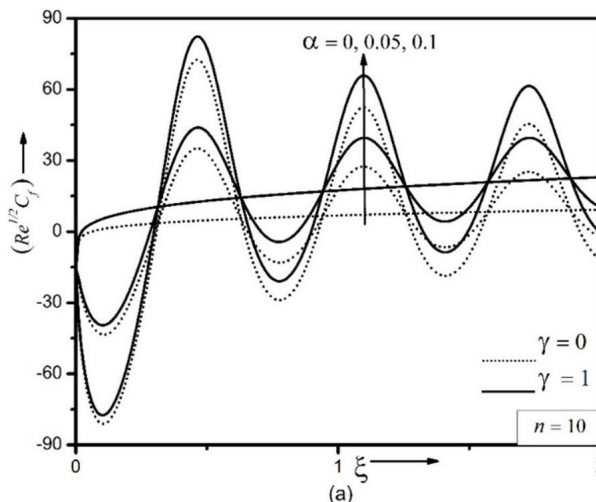


FIGURE 8. Effect of  $\alpha$  and  $\gamma$  on  $(Re^{1/2}C_f)$  for  $Pr = 7$ ,  $Ri = 10$ ,  $Re = 10$ ,  $Le = 10$ ,  $Nr = 0.1$ ,  $Ec = 0.1$ ,  $Nb = 0.1$ ,  $M = 0.1$ ,  $Nt = 0.1$ , and  $\varepsilon = 0.5$ .

### 4.3. Surface roughness and nonlinear mixed convection effects on gradients

#### 4.3.1. Skin-friction coefficient

The Fig. 8(a) - 8(b) show the variation of skin-friction coefficient  $(Re^{1/2}C_f)$  along  $\gamma$  for increasing values of small parameter  $\alpha$  and nonlinear mixed convection parameter  $\gamma$  for (a)  $n = 10$  and (b)  $n = 20$ , respectively.

For increasing values of  $\alpha$  and  $\gamma$ , the magnitude of skin-friction coefficient increases significantly. Moreover, the number of oscillations increase for higher values of  $n$ . Since the surface roughness is modelled with small amplitude and larger frequency sine waves, the small parameter  $\alpha$  indicates the depth of a sine wave, while the frequency parameter  $n$  signifies the number of cycles. Thus, for more values of  $\alpha$  and  $n$ , such variations can be found in the skin-friction coefficient. In addition to this, presence of nonlinear mixed convection ( $\gamma = 1$ ) increases the movement of fluid particles near the plate and this fact increases the friction at the wall.

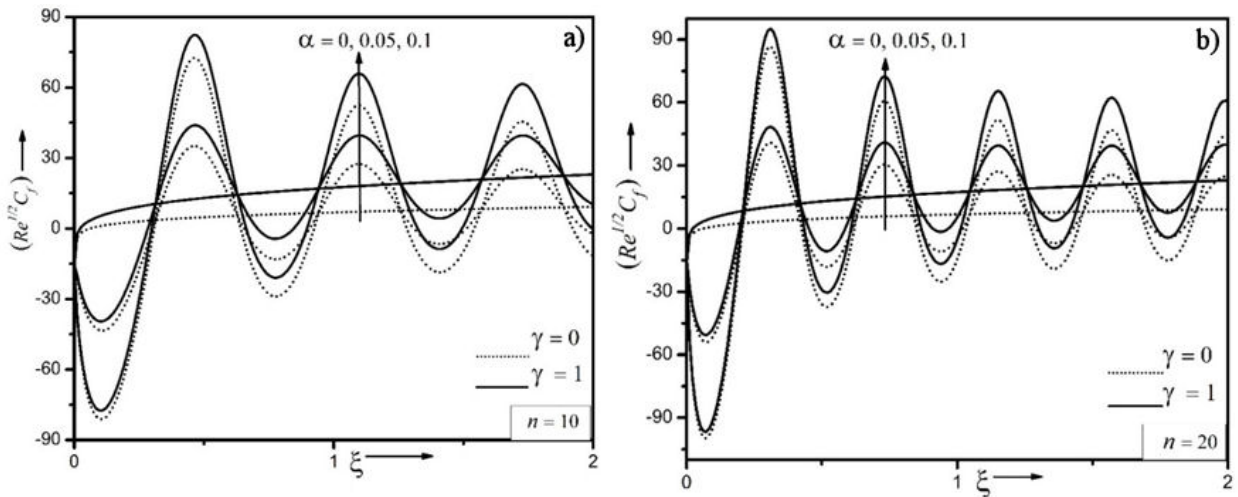


FIGURE 9. Effect of  $\alpha$  and  $\gamma$  on  $(Re^{-1/2}Nu)$  for  $Ri = 10, Re = 10, Pr = 7.0, Le = 10, Nr = 0.1, Nb = 0.1, Nt = 0.1, Ec = 0.1, M = 0.1,$  and  $\varepsilon = 0.5$ .

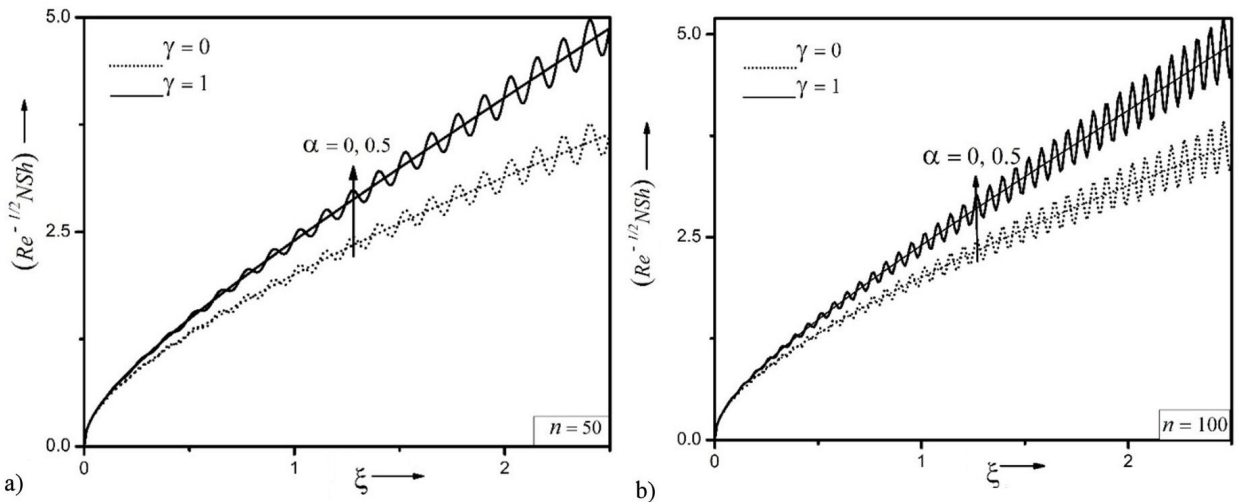


FIGURE 10. Effect of  $\alpha$  and  $\gamma$  on  $(Re^{-1/2}NSh)$  for  $Pr = 7.0, Ri = 10, Nt = 0.1, Re = 10, Le = 10, Nr = 0.1, Ec = 0.1, M = 0.1, Nb = 0.1,$  and  $\varepsilon = 0.5$ .

4.3.2. Wall heat transfer rate and nanoparticle mass transfer rate

Figures 9 and 10 portray, respectively, the sinusoidal variations of rate of heat transfer  $(Re^{-1/2}Nu)$  and nanoparticle mass transfer rate  $(Re^{-1/2}NSh)$  along  $\xi$  for various values of small parameter  $\alpha$ , nonlinear mixed convection parameter  $\gamma$  and frequency parameter  $n$ . The magnitude of rate of heat transfer and nanoparticle mass transfer rate increases for non-zero values of  $\alpha$  and  $\gamma$ . Also, the number of oscillations increases with larger value of  $n$ . The roughness at the plate creates more surface area and thereby helps to the process of transfer of heat in a larger quantity from the plate into the ambient fluid. On the other hand, the presence nonlinear mixed convection parameters ( $\gamma = 1$ ) reduces the the temperature of fluid and hence, assist to transfer of more heat from the plate into the fluid as compared to that in ab-

sence of nonlinear mixed convection parameter ( $\gamma = 0$ ). In addition to this, the higher values of  $\alpha, n$  indicate the wall with more surface area and which causes such variations in the nanoparticle mass transfer rate compared to absence of nonlinear mixed convection.

4.4. Comparison of heat transfer rate for in absence and presence of nanoparticles

Figure 11 illustrates the comparison between an ordinary fluid and a nanofluid in terms of heat transfer rate  $(Re^{-1/2}Nu)$  for both smooth as well as rough surfaces cases. The magnitude of rate of heat transfer for the nanofluid decreases as compared to an ordinary fluid. With the inclusion of nanoparticles into the base fluid, suspended nanoparticles accumulate at the hot plate and acquire enough heat energy. This process significantly reduces the transfer of heat from

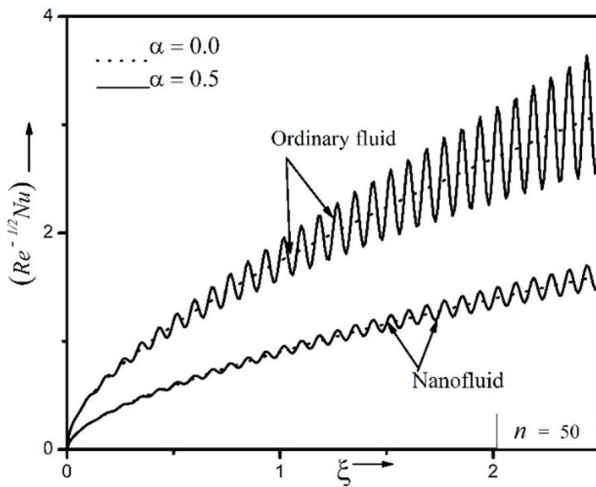


FIGURE 11. Effect  $\alpha$  on  $(Re^{-1/2}Nu)$  for  $Ri = 10, Re = 10, Pr = 7.0, Le = 10, Nr = 0.1, Ec = 0.1, M = 0.1, \alpha = 0.5, \varepsilon = 0.5,$  and  $\gamma = 0.1$ .

TABLE I. Comparison of heat transfer rate  $(Re^{-1/2}Nu)$  values obtained in the present analysis with the results of Minkowycz and Sparrow [14] and Mohamad, *et al.* [15] for various values of Richardson number  $Ri$  when  $\xi = 0, Re = 0, Nr = 0, Ec = 0, M = 0, Le = 0, Nb = 0, \varepsilon = 0, Nt = 0, \alpha = 0, n = 0,$  and  $\gamma = 0$ .

Ri	Minkowycz and Sparrow [14]	Mohamad, <i>et al.</i> [15]	Present results
0.0	0.29268	0.29266	0.29267
1.0	0.41054	0.41053	0.41053
2.5	0.48619	0.48617	0.48618
5.0	0.56067	0.56065	0.56066
7.0	0.60283	0.60282	0.60281
10.0	—	—	0.75927

the plate to the ambient fluid. For example, at  $\xi = 0.5$  the heat transfer rate reduces about 49 % for both rough as well as smooth surfaces in presence of nanoparticles.

The results established in the present study are validated by comparing the heat transfer rate  $(Re^{-1/2}Nu)$  with the previously established results of Minkowycz and Sparrow [14] and Mohamad *et al.* [15] in the Table I for different values of Richardson number  $Ri$  when  $\xi = 0, Re = 0, Nb = 0, Ec = 0, Nr = 0, M = 0, Le = 0, Nt = 0, \varepsilon = 0, \alpha = 0, n = 0,$  and  $\gamma = 0$ .

In Table II, the values of wall heat transfer rate  $|Re^{-1/2}Nu|$  and nanoparticle mass transfer rate  $|Re^{-1/2}NSh|$  are presented for the case of absence of nonlinear mixed convection parameter  $\gamma$  for both the cases of absence and presence of magnetic field parameter  $M$  and for smooth ( $\alpha = 0$ ) and rough ( $\alpha = 0.5$ ) surfaces.

Similarly, in the Table III, the values of wall heat transfer rate  $|Re^{-1/2}Nu|$  and nanoparticle mass transfer rate  $|Re^{-1/2}NSh|$  are presented for the case of presence of nonlinear mixed convection parameter  $\gamma$  for both the cases of

TABLE II. Wall heat transfer rate  $|Re^{-1/2}Nu|$  and nanoparticle mass transfer rate values for both the cases of absence and presence of magnetic field parameter  $M$  and for smooth ( $\alpha = 0$ ) and rough ( $\alpha = 0.5$ ) surfaces when  $\gamma = 0.5, Pr = 7.0, Ri = 10, Re = 10, Nt = 0.1, Ec = 0.1, Le = 10, Nr = 0.1, \varepsilon = 0.5, Nb = 0.1,$  and  $n = 50$  (Case of absence of nonlinear mixed convection parameter  $\gamma$ ).

Gradients	Absence of nonlinear mixed convection parameter ( $\gamma = 0$ )			
	$\alpha = 0$		$\alpha = 0.5$	
	$M = 0$	$M = 0.1$	$M = 0$	$M = 0.1$
$ Re^{-1/2}Nu $	0.58960	0.58650	0.59847	0.59533
$ Re^{-1/2}NSh $	1.31416	1.30850	1.33393	1.32831

TABLE III. Wall heat transfer rate  $|Re^{-1/2}Nu|$  and nanoparticle mass transfer rate  $|Re^{-1/2}NSh|$  values for in absence and presence of magnetic field parameter  $M$  and for smooth ( $\alpha = 0$ ) and rough ( $\alpha = 0.5$ ) surfaces when  $\xi = 0.5, Pr = 7.0, Ri = 10, Re = 10, Nt = 0.1, Ec = 0.1, Le = 10, Nr = 0.1, \varepsilon = 0.5, Nb = 0.1$  and  $n = 50$  (Case of presence of nonlinear mixed convection parameter  $\gamma$ ).

Gradients	Presence of nonlinear mixed convection parameter ( $\gamma = 1$ )			
	$\alpha = 0$		$\alpha = 0.5$	
	$M = 0$	$M = 0.1$	$M = 0$	$M = 0.1$
$ Re^{-1/2}Nu $	0.62341	0.61995	0.63278	0.62924
$ Re^{-1/2}NSh $	1.48604	1.48237	1.50751	1.50352

absence and presence of magnetic field parameter  $M$  and for smooth ( $\alpha = 0$ ) and rough ( $\alpha = 0.5$ ) surfaces. From Table II and Table III, it is noted that in presence of magnetic field parameter, the heat transfer rate and nanoparticle mass transfer rate decrease, while for in presence of rough surface and nonlinear mixed convection parameter,  $|Re^{-1/2}Nu|$  and  $|Re^{-1/2}NSh|$  increase significantly. This signifies that the increasing value of magnetic parameter, surface roughness parameter and nonlinear mixed convection parameter show prominent effect on the magnitude of heat transfer rate and nanoparticle mass transfer rate.

### 5. Conclusions

An innovative investigation of nonlinear combined convection nanofluid flow is carried out in presence of surface roughness and the following conclusions are summarized from the detailed analysis of MHD nonlinear mixed convection nanofluid flow along moving vertical rough plate:

- The magnitude of velocity profile increases and that of temperature profile decreases with the increase in values of non-similarity variable  $\xi$ . This signifies the influence of non-similar solutions.

- The magnitude of velocity profile increases for increasing values of nonlinear mixed convection parameter  $\gamma$ , while decreases for increasing values of nanoparticle buoyancy ratio parameter  $Nr$ .
- The increasing values of nonlinear mixed convection  $\gamma$  reduce the temperature profile, while the increasing values of thermophoresis parameter  $Nt$  increase the same.
- The higher values of Lewis number and nonlinear

mixed convection parameter reduces the nanoparticle volume fraction profile.

- The presence of magnetic field parameter  $M$  increases the magnitude of temperature profile, while decreases the magnitude of wall heat transfer rate.

## Acknowledgments

This work is supported by UGC-SAP-DRS-III with No. F. 510/3/DRS-III/2016 dated 29-02-2016.

1. P. C. Sinha, *Chem. Eng. Sci.* **24** (1969) 33-38.
2. K. Vajravelu and K. S. Sastri, *Int. J. Heat Mass Transf.* **20** (1977) 655-660.
3. S. S. Motsa, F. G. Awad, and M. Khumalo, *Abs. Appl. Anal.* **2014** (2014) 408230.
4. M. Bandaru, M. M. Rashidi, and H. Raju, *Therm. Sci.* **21** (2017) 2781-2793.
5. I. C. Mandal and S. Mukhopadhyay, *Mech. Adv. Mater. Struct.* **26** (2018) 2040-2046.
6. J. Taylor, A. Carrano, and S. Kandlikar, *Int. J. Therm. Sci.* **45** (2006) 962-968.
7. M. Ehsan, M. Salehin, and A. K. M. S. Islam, *Int. J. Auto. Mech. Eng.* **14** (2017) 4432-4447.
8. M. R. Salimpour, A. Abdollahi, and M. Afrand, *Exp. Therm. Fluid. Sci.* **88** (2017) 288-300.
9. Y. Pan, D. Jing, H. Zhang, and X. Zhao, *Entropy*, **20** (2018) 334.
10. S. U. S. Choi, in *Developments and applications of non-Newtonian flows 1995*, edited by D. A. Siginer and H. -P. Wang, (ASME, New York, 1995), Vol. FED231/MD66, pp. 99-105.
11. S. V. Subhashini and R. Sumathi, *Int. J. Heat. Mass. Transf.* **71** (2014) 117-124.
12. M. Sheikholeslami, S. A. Shehzad, A. Shafee, F. M. Abbasi, R. Kandasamy, and Z. Liig, *Rev. Mex. Fis.* **65** (2019) 365-372.
13. K. Ganesh Kumar, S. A. Shehzad, T. Ambreen, and M. I. Anwar, *Rev. Mex. Fis.* **65** (2019) 373-381.
14. W. J. Minkowycz and E. M. Sparrow, *Numer. Heat Tr. B Fund.* **1** (1978) 69-85.
15. R. Mohamad, R. Kandasamy, and M. Ismoen, *J. Appl. Comput. Math.* **4** (2015) 1000261-1000270.
16. P. M. Patil and I. Pop, *Heat Mass Transf.* **47** (2011) 1453-1464.
17. P. M. Patil, S. Roy and I. Pop, *Chem. Eng. Comm.* **200** (2013) 398-417.
18. P. M. Patil, A. Shashikant, S. Roy, and E. Momoniat, *Int. J. Heat Mass Transf.* **111** (2017) 643-650.
19. P. M. Patil, H. S. Ramane, S. Roy, V. Hindasageri, and E. Momoniat, *Int. J. Heat Mass Transf.* **104** (2017) 392-399.
20. H. R. Pasaribu and D. J. Schipper, *Tribol. Lett.* **17** (2004) 967-976.
21. H. Schlichting and K. Gersten, *Boundary-Layer Theory*, (Springer, New York, 2000).
22. P. M. Patil, S. Roy, R. J. Moitsheki, and E. Momoniat, *Heat Transf. Asian Res.* **46** (2017) 1087-1103.
23. P. M. Patil, D. N. Latha, S. Roy, and E. Momoniat, *Ain Shams Eng. J.* **8** (2017) 697-705.
24. J. Buongiorno, *ASME J. Heat Transf.* **128** (2006) 240-250.
25. P. R. Owen and W. R. Thompson, *J. Fluid. Mech.* **15** (1963) 321-324.
26. C. Ram Reddy, P. V. S. N. Murthy, A. J. Chamkha and A. M. Rashad, *Int. J. Heat Mass Transf.* **64** (2013) 384-392.
27. P. M. Patil, M. Roy, S. Roy, and E. Momoniat, *Int. J. Heat Mass. Transf.* **117** (2018) 287-295.
28. P. M. Patil, A. Shashikant, and P. S. Hiremath, *Int. J. Hydrog. Energy.* **43** (2018) 20101-20117.
29. R. S. Varga, *Matrix Iterative Analysis*, (Prentice-Hall, New Jersey, 2000).